Molecular Clouds as Ensembles of Transient Cores

R. T. Garrod,[1,2] D. A. Williams,[2] and J. M. C. Rawlings[2]

rgarrod@mps.ohio-state.edu

ABSTRACT

We construct models of molecular clouds that are considered as ensembles of transient cores. Each core is assumed to develop in the background gas of the cloud, grow to high density and decay into the background. The chemistry in each core responds to the dynamical state of the gas and to the gas-dust interaction. Ices are deposited on the dust grains in the core's dense phase, and this material is returned to the gas as the core expands to low density. The cores of the ensemble number typically one thousand and are placed randomly in position within the cloud, and are assigned a random evolutionary phase.

The models are used to generate molecular line contour maps of a typical dark cloud. These maps are found to represent extremely well the characteristic features of observed maps of the dark cloud L673, which has been observed at both low and high resolutions. The computed maps are found to exhibit the general morphology of the observed maps, and to generate similar sizes of emitting regions, molecular column densities, and the separations between peaks of emissions of various molecular species. The models give insight into the nature of molecular clouds and the dynamical processes occurring within them, and significantly constrain dynamical and chemical processes in the interstellar medium.

Subject headings: ISM: clouds — ISM: molecules — ISM: structure — ISM: individual (L673) — stars: formation

1. Introduction

There is now a large body of evidence showing that dark molecular clouds in the interstellar medium are clumpy on a scale not resolved by single-dish molecular line observations.

[1]Department of Physics, The Ohio State University, 191 West Woodruff Avenue, Columbus, OH 43210.

[2]Department of Physics and Astronomy, University College London, Gower Street, London, WC1E 6BT, UK.

For example, Peng et al. (1998) showed from CO line observations that the well-studied TMC-1 Core D, previously regarded as a single entity in dynamics and chemistry, consists of some 47 distinct sub-cores. This notable discovery has beeen shown to have implications for the evolution of TMC-1 and its chemical richness (Hartquist et al. 2001). Morata et al. (2003) used the BIMA interferometer to make a detailed study of structure within the molecular cloud L673. Their maps in lines of CS, N_2H^+, and HCO^+ showed considerable structure not previously revealed in single-dish studies (Morata et al. 1997). This structure is different in each molecular line, suggesting that chemical time-dependence is responsible, and that the density inhomogeneities (hereafter described as cores) are probably growing from low to high density on a time-scale around one million years and then dissipating on a similar time-scale. Further work by Morata et al. (2005) combined both single-dish and array observations, and the resulting maps which represented emissions from both background and clumped gas confirmed the general picture of Morata et al. (2003).

This small-scale structure had, in fact, been inferred a decade earlier from observations of (particularly) CS and NH_3 lines in a number of objects (Myers et al. 1991; Morata et al. 1997); these studies showed unexpected distributions in the emissions from these molecules. Taylor et al. (1996) proposed that the unexpected behaviour could be understood on the basis of time-dependent chemistry in unresolved structures that grow and decay on time-scales of around a million years. Alternative explanations were also offered (see section 3.2), but the interpretation of Taylor et al. (1996) now appears to be supported by the high-resolution observations of - so far - two molecular clouds. However, the general picture of clumpiness indicated by Peng et al. (1998) and by Morata et al. (2003, 2005) is also supported by discussions of the chemistry associated with interstellar clumpiness (Cecchi-Pestellini & Dalgarno 2000) and extending to very small and very transient structures in diffuse interstellar clouds (Hartquist et al. 2003).

Garrod et al. (2005, hereafter GWHRV) modelled the chemistry of a single transient core within a cloud. They assumed that the clump grows from a low density background gas to high density and then decays into the background according to a prescription based on a study by Falle & Hartquist (2002) of the passage of MHD waves through a partly ionized cloud (other authors have also found density inhomogeneities may be produced in low-beta plasma conditions, based on turbulence simulations, see e.g. Elmegreen 1999, and references therein). In this model, the chemistry follows the changing density as a function of position within the core; ices form on dust in the denser parts of the core and are returned to the gas phase when the density decreases. The main conclusions of GWHRV were that the dynamical time-dependence and the gas grain interactions greatly affected the chemistry as compared to that in more conventional models based on static objects.

In the present paper we adopt the picture of molecular clouds established observationally for TMC-1 Core D and for L673; i.e. we assume that a molecular cloud may be considered as an ensemble of transient cores. The observations indicate that a range of core masses is present. For simplicity, however, we assume in the present work that all cores have the same mass; alternative pictures will be investigated in later work. We use the chemical results of GWHRV for a single core, and create synthetic maps at both low and high resolution of an idealized molecular cloud composed of a large number of such transient cores. These cores are positioned randomly within our model cloud, and are taken to be at random stages of evolution in the cycle from low to high density and back again. Our aim in creating these maps is to determine whether such a model of a molecular cloud is better able to represent the observed properties of molecular clouds than conventional static and uniform models, and to use these models to throw light on the dynamics, chemistry, and gas-grain interactions occurring in these clouds. Note that we do not attempt here to model a specific cloud in this work.

In Section 2 we describe the chemical model of a single core used in this work, the method of map generation and the map parameters adopted. In Section 3 we present results in the form of high and low resolution contour maps of emissions from various molecules for our model cloud. These show remarkable similarity to observational maps. In Sections 4 and 5 we consider the stability of our conclusions with respect to changes in map parameters and to the adopted mantle re-injection properties. Our general conclusions are presented in Section 6.

2. The Model and Assumptions

2.1. The Chemical Model

We assume that the synthetic dark cloud region is made up entirely of cores with the chemical and physical parameters of a single generic standard core, similar to that of the standard run of GWHRV. The new standard core differs slightly from GWHRV in several ways:

- The number of species is increased by 30, to 251. The new chemical species consist mainly of longer carbon chain molecules (up to five carbon atoms compared to three).
- The level of freeze-out is parametrised in a different way; rather than setting fr, the freeze out *rate*, to a standard value, it is set such that it will produce a standard percentage of CO freeze-out for the central depth point at the time when peak density

is achieved. This level is chosen to be 60%. We therefore identify 60% CO freeze-out with a sticking coefficient of unity.

- We choose a threshold visual extinction for freeze-out to proceed of $A_{V,crit} = 2.5$. The original value of 2 was set to ensure that freeze-out would have *some* noticeable effect; since this is quite clearly not a problem, we choose a new value more in keeping with the estimate from Whittet et al. (2001) of between 2 and 3. This has the effect of limiting freeze-out to depth points 7 - 12 (cf. points 6 - 12 in GWHRV).

- We choose a peak central visual extinction of exactly 5.0 rather than 5.12.

This model produces the same general features as GWHRV, with the following differences: the higher level of freeze-out results in slightly higher grain mantle abundances of CO, and higher gas phase levels of NH_3, CH_4 and other less abundant carbon-bearing molecules, at earlier times. CS shows the same double-peaked structure as before, but shows stronger central depletion. By the end of the run, any differences have largely disappeared.

Previous modelling runs have shown that the chemistry of the core is not strongly sensitive to a change in evolution time-scale of a factor of two shorter or longer, hence our adoption of one core evolution time-scale to represent all cores is acceptable.

An example of the results from the model is shown in figures 1a & b. The discontinuities in the column density profiles after peak time are a numerical artefact; the result of the discrete placement of chemical reference points in the core, and follow from the instantaneous re-injection of grain ice mantles into the gas phase (as discussed in GWHRV). We have remedied this numerical problem by integrating the profiles between the peaks, effectively eliminating the artificial peak structure (figures 2a & b).

This procedure is not entirely consistent with the chemistry, since with a continuous distribution of reference points throughout the core, we should expect the levels at each point to combine with the others, producing larger overall levels. However, the rate of re-injection and the range of visual extinctions over which it may take place is not known, since the mechanism itself is not understood. We therefore consider two extremes: smoothed column density profiles at the peak values should reasonably produce a maximal re-injection peak effect. Conversely, by smoothing over the peaks by integrating between the levels obtained before the peaks occur and after they have relaxed, we may obtain profiles for a minimal level of re-injection. This approximates the case where re-injection is slow compared to gas phase reactions. We investigate this case in section 5.

We make no attempt to model the details of the radiative transfer, and do not consider optical depth effects. However, we incorporate a very approximate treatment of the exci-

tation: We may simplistically argue that for emission in a molecular line to be detectable, the gas density must be above the critical density for thermalisation (see e.g. Evans 1989). However, as explained in Evans (1989), a more realistic effective critical density (n_{eff}) which takes into account such processes as multi-level transitions and the trapping of line photons in optically thick lines, can be defined. Evans (1999) presents values of n_{eff} (defined to be the value of the density which yields a line strength of 1K in the relevant transition) calculated using a large velocity gradient radiative transfer code for some commonly observed molecular transitions, and adopting a kinetic temperature of $T_{\rm K} = 10$ K (see Table 1).

We adopt these threshold values and employ them in the calculation of column densities using the value of n_{eff} as an integration edge, so that material in the core for which $n_{\rm H} \geq n_{\mathit{eff}}$ contributes to the emission, whilst material with $n_{\rm H} < n_{\mathit{eff}}$ does not. This approach is still quite simplistic, but acts to limit contributions from highly extended regions of gas which may not be of sufficient density to emit. This will mostly affect CS morphologies in the synthetic maps, since the CS (J=2→1) line, used in Morata et al. (2003), has a high value of n_{eff}. CS is abundant in relatively low density cores at early/late times; the effect should heavily subdue contributions from these cores in the CS (J=2→1) line, and should cut down the calculated levels even in cores at peak densities.

The critical densities and other information for relevant transitions are shown in Table 1 (Evans 1999). Note that data for N_2H^+ were not available. For CO, we assume that a gas density of 1000 cm^{-3} is sufficient to produce a detection (Ungerechts et al. 1997), since the small dipole moment of the CO molecule produces lines that are usually very well thermalised.

Figure 2a shows the unsmoothed column density profiles obtained using the effective critical densities of Table 1. Figure 2b shows the smoothed profiles. Note that CS and NH_3 are by far the most strongly affected by re-injection. The CS (J=2→1) transition may be seen to trace the cores at closer to the peak density than the CS (J=1→0) transition, although the column densities produced are a little lower. The figures show clearly at what stage in a core's evolution the densities are too low to produce detectable emission in the CS transitions.

2.2. The morphological model

Having established a chemical model for an individual core, we subsequently assume that each core has identical chemical and physical/dynamical parameters. The only free parameters are the location and evolutionary status of the cores. To each core we therefore

assign column densities calculated for all the molecules modelled in the standard run, which vary depending on the designated stage of evolution of each core. To construct a map of the ensemble of cores we adopt the following approach:

- Designate a map size, and the number of cores within it
- Assign each core a randomly determined position
- Assign each core a randomly determined stage of evolution

Note that there is no empirical constraint, or model significance, concerning the location of the cores in the third dimension.

This results in a purely random ensemble of cores, with no inherent bias towards any particular structure other than that the region is composed of discrete cores of gas, and that a uniform core number density has been adopted for the whole region. This is consistent with the apparent lack of any particular bias in the L673 region. There will, however, be an effect on the resultant local morphologies displayed within the maps from groupings resulting from the random distribution of the cores. This will result in unique morphologies for any given distribution of cores.

We also make the important assumption that the cores are chemically and physically non-interacting. This is also consistent with the observations of individual cores and the findings of the theoretical models. In any case, those cores which are localised in the plane of the map may not in fact be close neighbours in three dimensions.

We then convolve the integrated column densities of each core into a set of molecular line maps for various tracers:

- *Divide map into a grid of "detection points".*
  The resolution of the grid of reference points must be smaller than the beam resolution so that the entire map is well covered by the simulated beam.
- *Designate a beam resolution/beam width.*
  A beam resolution is chosen which simulates a real telescope. A simple Gaussian diffraction profile is assumed for the beam.
- *For each detection point, calculate contribution of "detected column density" from each core which lies within the detection radius.*
  In this way, simulated detection levels are attributed to each detection point in the map from which contour maps can be generated.

To characterize the size of the cores, we adopt a Gaussian profile, and define a scale width as the intrinsic radius. Since the models of Falle & Hartquist (2002) are only one-dimensional, we cannot say with any certainty how the density profiles along other axes may vary. However, the adoption of a Gaussian profile is in line with the density profile approximations along the axis of core collapse. We make one further constraint on the intrinsic radius of the core: that it obeys the conservation of mass requirement (GWHRV). The Falle & Hartquist (2002) mechanism does not necessarily require the cores to conserve their mass, however this stipulation is in line with our assertion that the cores are individual, non-interacting entities. Because all of the column density calculations obtained from the chemical model are made along the principal collapse axis, for the sake of consistency we assume that each core is aligned with its principal collapse axis along the line of sight. Therefore, we allow the observed radius of each core to vary only in a way consistent with this alignment, that is:

$$\Delta r(t) \propto [\Delta z(t)]^{1/4}$$

where $\Delta z(t)$ is the core scale width along the principal axis as defined in GWHRV (see Appendix for derivation) and is calculated in the chemical model. $\Delta r(t)$ obviously reaches a minimum at the time of the peak density of the core, t_m. We fix $\Delta r(t_m)$ so that it assumes a value of some (substantial) fraction of $\Delta z(t_m)$, determined according to comparisons with Morata et al. (2003).

Having attributed each core with an intrinsic width dependent on its stage of evolution, the map of the cores of finite dimensions is convolved with the (off-axis) Gaussian beam to produce the synthesized maps. Note that the column densities only account for the centre of the core, along the line of sight, so the "detected" morphologies should be thought of as being representative of the extents of the *core centers* rather than the entire core plus envelope.

The uniform alignment of the cores' collapse axes along the line of sight is a necessary simplification, given the 1-dimensional nature of reliable MHD simulations (see GWHRV; Falle 2002) on which to base our dynamical model. The main effect of this assumption is to make every core circular in the plane of "observation"; we might expect that a full 3-dimensional chemical/dynamical model would produce non-circular morphologies for individual cores, if even higher resolutions than we use here were adopted. It should not have a drastic effect on the convolved morpholgies shown in this work. We would also expect that the relative extents in the plane for molecules in individual cores could be somewhat different (e.g. CS versus NH_3; see the collapse-axis molecular extents shown in GWHRV). However, this effect should not be large since contributions are strongest from the core centers. It could be remedied by choosing core widths according to the molecule being mapped, however for consistency we use the same widths for all molecules.

2.3. The Adopted Map Parameters

There are approximately 40 spatially separable cores observed in the CS (J=2→1) line in the ∼(0.5 pc)^2 maps of Morata et al. (2003). The cores observed in the HCO^+ (J=1→0) and N_2H^+ (J=1→0) lines do not generally coincide with those of CS or with each other; this is as expected (GWHRV) and is primarily a result of chemical differentiation within the cores. Also, some closely separated cores will be unresolved whilst others will have observationally undetectable column densities. We therefore estimate a value of ∼60 cores, leading to a core number density of 250 pc^{-2}.

We use a global map size of 2 pc×2 pc (approximately equal to the size of the CS maps of Morata et al. 1997) within which there are a total of 1000 cores. Figure 3 shows the basic map of core positions, the synthetic "sky". We denote the approximate stage of evolution: Plusses (+) indicate cores that have not yet reached peak time, and are therefore not yet at maximal density; crosses (×) indicate cores which have evolved past the peak time. The relative sizes of the symbols also indicate approximately how far into the cycle the cores are: larger symbols indicate larger densities (or proximity to peak time).

We take two subsets of the data in these maps which simulate the observational data:

- *Large-scale, low resolution maps.*
  These maps essentially cover the whole 2pc×2pc area, although we ignore "emission" from within 0.1 pc of the edges. This is because levels at the edges are influenced by the lack of any cores outside of the map, producing an unnatural drop in "detection". To avoid this artefact, we remove a strip around the edge of the maps of size approximately equal to the beam radius. The resolution corresponds to a beam width of just under 2 arcmin to agree approximately with Morata et al. (1997). This corresponds to a beam radius of 0.085 pc, calculated at a distance to L673 of 300 pc.

- *Small-scale, high resolution maps.*
  Here we zoom in on a region of the low resolution maps of size ∼ 0.6 pc × 0.6 pc chosen so as to accommodate both local CS and NH_3 peaks. This is comparable to the area (∼0.5 pc × 0.5 pc) studied by Morata et al. (2003). This was chosen from within the detection map of Morata et al. (1997) to coincide with peaks in CS emission, and in NH_3 detected by Sepúlveda Cerrada (2001).

  The synthesised beams employed in Morata et al. (2003) using BIMA are ∼ 20 × 15 arcsec, corresponding to a circular beam radius used here of ∼0.0125 pc.

Note that a single beam width is adopted for all species/transitions.

3. Results

3.1. Low resolution, large-scale maps

Figures 4a – f show low resolution (∼2' FWHM) *column density* convolved molecular line maps for six density tracers. We overlay the basic map of core positions (Fig. 3) for ease of comparison. The contours represent fractions of the peak value calculated for the map, for any particular molecule. The fractions of peak "emission" represented by the contours are chosen to correspond with those of the low resolution observations shown in Morata et al. (2003). The outermost (thick) contour line represents the half-maximum (0.5), with the levels rising by ∼0.05. The overlaid boxes represent the portion of the map on which we zoom-in in the high resolution maps.

As is generally observed in dark clouds (see e.g. Myers et al. 1991) the morphologies of the different molecular tracers are not the same, do not trace the same regions, and have different spatial extents. Indeed we see here that the characteristic features exhibited in molecular line maps of CO, CS and NH_3 in Myers et al. (1991) are broadly re-produced. We find that CO and CS are not significantly different in spatial extent. The "detection" of NH_3 is comparatively compact and agrees well with the evidence of Myers et al. (1991). HCO^+ and N_2H^+ both seem to track approximately the same regions of gas, with very similar morphologies and extents. These molecules display smaller extents than CO or CS and their contour map peaks correspond to peaks in H_2 and CO. This is consistent with the observation that N_2H^+ tends to be a good density tracer.

3.2. High resolution, small-scale maps

For the zoomed-in high resolution synthetic molecular line maps, we choose a region from the bottom-left section of the map of approximately the same size as the region of L673 examined in Morata et al. (2003), chosen for the presence of CS and NH_3 peaks in that area.

Figures 5a – f show maps for CO, CS, HCO^+, NH_3 and N_2H^+. Contour levels are set to correspond to those used in Morata et al. (2003): the lowest is 0.36 of maximum, the others increasing by 0.07.

In comparison with Morata et al. (2003), the CS morphologies are generally similar, although we do not see so many resolved cores in the synthetic map; the same is true for HCO^+. Although the overall morphology for N_2H^+ is very similar to that of HCO^+, the number of resolved N_2H^+ cores matches well with Morata et al. (2003). Both the larger- and

smaller-sized cores are reproduced in the synthetic maps. Note that the "emission" is not purely centred around individual cores but around small groupings. Clumps of emission out on their own which reach only two or three contour levels (0.43 – 0.50 of maximum) tend to be the result of individual cores or loose associations of two or three.

The good agreement of comparative CS and NH_3 peak positions and extents in the low resolution maps with the observational evidence of Morata et al. (1997) is encouraging: The general morphologies of these molecules match those of dark cloud cores examined in Myers et al. (1991). Those authors calculated mean FWHM extents in 16 dark cloud cores to be 0.15 pc (NH_3), 0.27 pc (CS) and 0.36 pc ($C^{18}O$). The extents of CS and NH_3 are arguably larger than this, but appear to preserve the correct relative extents. This is particularly important in that the spatial extents of the CS and NH_3 emissions are the opposite of what one would expect from simple critical density arguments *for a single core* (see e.g. Rawlings 1996). Previous attempts to resolve this problem (e.g. Tafalla et al. 2002) have invoked differential depletion effects between sulphur-bearing and nitrogen-bearing species (following Bergin & Langer 1997), but the chemical basis for such models has not been confirmed.

Taylor et al. (1996) first suggested that the CS/NH_3 discrepancy could be a result of the clumpy nature of molecular clouds. Their chemical models used the modified free-fall collapse mechanism of Rawlings et al. (1992), and did not include subsequent dispersal. They conjectured that most clumps would disperse before significant NH_3 levels could build up, whilst CS should peak before this time arrived. The adoption of the mechanism proposed by Falle & Hartquist (2002), here, allows for the (controlled) dispersal of a core. However it is for similar reasons as those suggested by Taylor et al. (1996) that the differences in the morphologies of CS & NH_3 is reproduced in our models; the NH_3 peaks later than CS, and for a less extended period of time.

The good morphological agreement of the high resolution maps, especially for N_2H^+, with those of Morata et al. (2003) indicates that the Falle & Hartquist (2002) mechanism produces data consistent with observations of small, transient, dense cores. Whilst the simulated low resolution maps should not be expected to correspond closely with the particular example of region L673, we note that, as in L673, the emission from CS and HCO^+/N_2H^+ do not generally represent the same cores, regions of stronger emission overlap, and similar ratios of strongly and weakly emitting cores are present.

In Table 2 we present column densities (and ratios) as determined by the model, for the low resolution and high resolution maps, and compare with levels detected in Morata et al. (1997) and Morata et al. (2003). Taking a similar approach to the latter work, we select the peak position for each transition in the high resolution maps and compare values at the same spatial positions. These points are represented by *diamond*-shaped markers in

figures 5b–e. We also give column density values calculated from the low resolution data, at the low resolution molecular line maxima within the high resolution map domain. These are represented by *square*-shaped markers. Following Morata et al. (1997), for each low resolution peak we present the column density only of the molecule whose peak it is. Peak A corresponds to the shared high resolution peak in CO and CS (J=1→0). Peaks B, C, and D correspond to the high resolution peaks in CS (J=2→1), HCO^+ (J=1→0) and NH_3 (1,1), respectively.

In Table 3 we present the equivalent column density data obtained from the low resolution observations of Morata et al. (1997) (their table 4) and the high resolution observations of Morata et al. (2003) (their table 3). Peaks E and W correspond to CS (J=2→1) peaks, whilst peak N corresponds to HCO^+ (J=1→0) and peak S to N_2H^+ (J=1→0).

Considering the low resolution peaks in Table 2; the CS (J=2→1) maximum (B) is close in value to the CS (J=1→0) peak level (A) - and the two peaks are located very close together. The low resolution HCO^+ value is more than an order of magnitude lower than the peak in either of the CS transitions. NH_3 is a factor of 2 – 3 lower than the CS peak levels. The distance between the NH_3 and CS (J=1→0) low resolution peaks is 0.31 pc, which agrees reasonably well with the $\sim$ 0.2 pc quoted for the specific case of L673 in Morata et al. (1997). However, the actual levels and ratios detected do not agree well with that paper. Whilst the synthesised NH_3 peak level may be as low as half the observed value, the synthesised CS (J=1→0) peak level is about an order of magnitude too high. This leaves a ratio of $[CS/NH_3]$=3.0, rather than the quoted value of ≤ 0.11.

For the high resolution synthetic values, at the CS (J=2→1) peak (B), the HCO^+ (J=1→0) column density is little changed from its peak value (C). However, the CS (J=2→1) column density at peak C is a factor of three lower than at B. This difference is due to peak B being an unresolved combination of three strongly emitting cores – one slightly post-peak density, another slightly pre-peak density, and the other a little younger again. This combination acts to give high values for each of the molecules except NH_3 (which is so strongly weighted towards later times in the column density profile of figure 2). The close proximity of the three cores, which are approximately 1 high resolution FWHM beamwidth apart, allows them to reinforce each other effectively.

The high resolution synthesised CS (J=2→1) and HCO^+ (J=1→0) column densities are even larger again than the observed values – peak CS levels are as much as two orders of magnitude larger than observed, and HCO^+ levels more than one order of magnitude larger. It can be seen that, contrary to the observations, the synthesised column densities are higher at the high resolution peaks than for the low resolution peaks. This is possibly an effect of the presence of many, unresolved, low-level cores in L673, or else the interferometric

observations may have resolved out the more extended features.

The overall column density levels obtained are generally too high, even at low resolution. Four factors may explain this: (i) the level of uniformity of core distribution may have an effect such that the peaks observed in the synthetic maps represent close associations of cores (as mentioned above), in particular those close associations of cores at similar stages of evolution, (ii) the chemical (and/or physical) evolution of individual cores may vary from that adopted here, (iii) this approach uses only one core chemistry to model the entire region. In reality, we might expect to see a spectrum of cores within the same cloud. Chemical model runs adopting different parameters from those of the standard core run have shown that the resultant chemistry (and the CS & NH_3 abundances) can vary strongly with visual extinction, (iv) smaller core widths (in the plane) should produce smaller column densities. The Morata et al. (2003) HCO^+ emission is less extended and more defined than the CS in particular, and this may be due to only smaller regions near the core centre being able to produce it. Evidently, the model cloud is chemically richer than L673. No attempt has been made here to model L673, other than in general morphology. It may be, for example, that the cosmic ray ionization rate is less for L673 than adopted in the model.

4. Testing the Effects of the Variation of Core Distribution

As suggested above, the precise morphological distributions depend on the assumed (random) distribution of the cores. In this section we investigate the sensitivity of the results to this distribution. We restrict the analysis to the high resolution maps so that the assumed distribution is locally valid.

We define two statistical measures of the uniformity of the distribution of the cores: the mean shortest inter-cores distance (ICD, analogous to core number density) and the standard error in this mean (SEM, uniformity of distribution). In the locality of a single core, the ICD is very important for the relative influences of either core on the convolved map, especially when close to the beam resolution limit. Higher values of the SEM imply greater deviations from uniformity.

We start by generating a quasi-random map with a very uniform distribution, and then stochastically move the positions of the cores by small amounts to vary the two statistical parameters. This results in maps whose only difference is in the location of cores, rather than their evolutionary status. Three cores distributions have been considered; (1): ICD=0.524 pc, SEM=4.21%, (2) ICD=0.520 pc, SEM=4.85%, and (3) ICD=0.529 pc, SEM=5.19%. The convolved molecular line maps for distribution (1) are shown in Figure 6.

Even with the much greater level of uniformity in distribution 1, we do not resolve many cores individually. We may discern, however, that for CO those peaks whose contours are very tight tend to be the result of core associations, whereas peaks whose contours are broad and fairly regular tend to be single cores, close to their peak densities. These peaks do not tend to be as strong as those for which core associations are responsible. For the other molecules, most peaks tend to be the result of the resolution of single, fairly isolated cores.

In general we find that the apparent degree of confusion in the maps is smaller and the peak levels and contrasts are larger for the more random (less uniform) distributions. The spacing between emitting cores is the dominant factor in determining the morphologies of the maps.

Using the different molecular tracers as test cases for these variables, we see that as in the case of the CS (J=2→1) maps, widely spaced emitting cores produce quite tight peaks, and more strong peaks tend to be present with decreasing uniformity of general core distribution.

Table 4 shows column densities at the peak positions (for the strongest peak in the map) for each molecule. It might seem that there is a slight trend for levels to be higher for lower uniformity of core distributions, but this is only consistently true for CO. However, this does suggest firstly that the levels obtained from observations are quite robust with respect to the pattern of core distribution, and secondly that the discrepancy between the observed and modelled CS/NH_3 column densities is not likely to be resolved by consideration of such effects.

The observed CS J=2→1 morphologies (Morata et al. 2003) most closely resemble the modelled morphologies of CO, particularly for the most uniform distribution, suggesting that CS cores are not highly clustered in L673, and that the contributing cores in that region are probably more numerous than is assumed in this model. The most probable explanation for this is that there are a number of inherently more weakly emitting cores in L673, which have different physical conditions from those that we have modelled. From the similarity between the modelled CO and the observed CS, we may infer that the E and W peaks in the CS (J=2→1) emission of Morata et al. (2003) are more likely to be the result of core associations, whilst the emission at peak N may come from two underlying cores.

5. Molecular Line Maps with Different Grain Mantle Re-injection Characteristics

Finally, we consider the effects of using column density profiles with a minimal contribution from the re-injection of dust grain mantles. This follows from the situation where the rate of deposition of grain mantle-bound species is so slow compared to the rate of destruction of injected species by the gas phase chemistry that there is no discernible difference in the resultant column density measured through the core. Figure 7 shows the resultant column density profiles and can be compared to the 'maximal' re-injection case (Fig. 2b). We apply these profiles to the same basic "sky" map.

Of the various tracers, the most strongly affected is the NH_3 morphology, shown in figure 8. It not only assumes a smaller spatial extent but maps different material from the maximal re-injection case - tracing regions that are very similar to those traced by HCO^+ (J=1→0). The relative morphologies of CS (J=1→0), CO and NH_3 (1,1) are perhaps closer to those observed by Myers et al. (1991) than in the maximal re-injection case.

However, the absolute NH_3 peak levels are less consistent with measured values. Since the absolute NH_3 column densities are a more robust measure, it is more likely that the morphologies exhibited in Myers et al. (1991) etc. are the product of a range of chemistries engendered by a spectrum of cores in dark clouds, as already discussed, rather than being explained purely by the adoption of the minimal re-injection profile.

High resolution maps show that the differences are slight compared to the maximal re-injection case for all species except NH_3, which maps very similar regions to HCO^+ (J=1→0) as at low resolution. Therefore, a test of this extreme of re-injection would be whether or not HCO^+ and NH_3 appear to map the same regions.

6. Summary and Conclusions

We have constructed a molecular line contour map of a model dark cloud by placing a large number of evolving cores randomly in space and attributing to each a randomly determined stage of evolution. The column density data from the chemical model of such an evolving core have been applied to each core in the map, and all such data convolved to simulate molecular line maps of dark cloud regions. Observational evidence of L673 from Morata et al. (1997 and 2003) has been used to guide the choice of map parameters.

The computed low resolution morphologies of NH_3 and CS are found to agree well with the observational evidence of the spatial extent of these molecules and with the relative

positions of peaks and contours in L673. CO assumes a slightly smaller extent than is evidenced by the survey of Myers et al. (1991) of 16 dark cloud cores.

The computed high resolution maps confirm that the model produces morphologies and peak positions similar to those in L673. The comparison of the synthetic maps with observational data suggests that the cores in L673 are randomly situated and have no particular bias in space.

We show in Sections 4 and 5 that the general behaviour of the model is fairly stable against variations in the spatial distribution of cores and the method of injection of ices into the gas phase during the expansion of the core.

The absence of proper radiative transfer in the code was a necessary compromise in our calculations, but the use of effective critical emission densities allowed the discrimination of different molecular line transitions in the simulations: The convolution of data obtained from chemical modelling to produce maps similar to observations is striking, and probably unique in the history of chemical modelling of molecular clouds. The level of agreement between observations and models of absolute values of molecular column densities is good and indicates that our proposal to model dark clouds as an ensemble of identical transient cores is not merely plausible but may actually represent the true situation.

In summary, our main conclusions from this study are as follows:

1. A molecular cloud model considered as a large ensemble of randomly placed evolving cores, each with randomly allocated states of evolution, generates molecular line maps at low and high resolution that are remarkably similar in character to those observed in L673; the observed structures cannot be generated by simple models of unitary homogeneous or collapsing clouds.

2. The molecular line maps broadly reproduce morphologies, sizes of emitting regions, and separation in peak positions in various species, as found in L673.

3. In such a model, the chemistry in each core responds to the changing physical state of the gas as it contracts from low density to a transient high density state and then back to low density. For the model to generate molecular line maps similar to those observed, the time-scale for the dynamical cycle is required to be on the order of a million years. This conclusion is consistent with the theoretical MHD study of Falle and Hartquist (2002).

4. The gas-dust interactions significantly affect the chemistry of each core and of the cloud. For the model to match observations, the freeze-out of gas-phase species that

occurs in the denser part of the cycle must remove a significant amount of matter (other than hydrogen and helium) from the gas (on the order of one half) in the form of ice mantles. The ice mantles must be returned to the gas as the core expands to a low density state.

5. The excellent morphological match of models with observational maps of L673 supports the view that the cores in that cloud are randomly spaced and randomly evolving, rather than being structured either spatially or temporally.

6. The contrast between CS and NH_3 distributions in L673 (and many other dark clouds; Morata et al. 1997) is well accounted for in the model. This justifies the assertion of Taylor et al. (1996) concerning unresolved cores. However, the extent of the model NH_3 emitting region is to some extent an artefact of the method of computing the injection of ices into the gas.

7. Our models clearly indicate that HCO^+ and N_2H^+ emissions should be co-located in the maps, contrary to the findings of Morata et al. (2003). However, their conclusion is that this may be an observational artefact: Morata et al. (2005) have shown that the apparent separation of HCO^+ and N_2H^+ emissions may be caused by high optical depths in the HCO^+ lines.

8. Observations of co-located emission peaks in CS and HCO^+ are predicted by the model to arise from superpositions of cores at different stages of evolution.

Finally, we emphasise that in the present models all the cores are assumed to have equal mass. It is clear, however, from the observations of Morata et al. (2003) that a range of core masses is present in L673. As larger cores evolve, they may become unstable to gravitational collapse. In future work, we shall consider the chemical implications of core size and the possible relation to low mass star formation.

R. T. G. thanks PPARC for a studentship, and the National Science Foundation for partial support. D. A. W. acknowledges the support of a Leverhulme Trust Emeritus Fellowship.

A. Appendix

In Garrod et al. (2005) the time- and depth-dependent density of each of the 12 chemical reference points is defined according to

$$\rho(\alpha, t) = \rho(0, t_m) \exp\left[-\alpha^2\right] \exp\left[-\left(\frac{t - t_m}{\tau}\right)^2\right] \tag{A1}$$

where t is time, t_m is the "peak time" at which density is maximal (half way through evolution), α is the parametrized distance from the center of the core, and $\rho(0, t_m)$ is the peak time central density. τ is defined according to the choice of the initial density at the core center (10^3 cm^{-3}) and the maximum density at the core centre, $\rho(0, t_m)$ (5×10^4 cm^{-3}). The distance of a parcel of gas from the center of the mass-conserved core is defined by

$$z(t) = \alpha.\Delta z(t) \tag{A2}$$

$$\Delta z(t) = \left[\frac{\rho(0,t_m)}{\rho(0,t)}\right]^{\frac{1}{k}} \Delta z(t_m) \tag{A3}$$

where $\Delta z(t)$ is the scale width at that time, and k represents the number of dimensions along which collapse is taking place.

If $\Delta z(t)$ represents the scale width of the core along the principal axis of collapse (along the line of sight), and assuming that the rates of collapse along the other two axes are equal (in the absence of other information), we may assign a core with a time-dependent radius in the plane of observation (representing scale width for a Gaussian function), $\Delta r(t)$. We may relate these quantities to the total mass of a core via:

$$M_{tot} \propto \rho(t).V \propto \rho(t).\Delta z(t).[\Delta r(t)]^2$$

Since the total mass is conserved, we have that:

$$\Delta z(t).[\Delta r(t)]^2 \propto [\rho(t)]^{-1}$$

Therefore, eliminating $\Delta z(t)$ using equation (A3):

$$\Delta r(t) \propto [\rho(t)]^{(\frac{1}{k}-1)/2}$$

Or, eliminating $\rho(t)$:

$$\Delta r(t) \propto [\Delta z(t)]^{(k-1)/2}$$

For the standard run which we use to construct the maps, $k = 1.5$ (see Garrod et al. 2005), hence:

$$\Delta r(t) \propto [\Delta z(t)]^{1/4}$$

REFERENCES

Bergin, E. A., & Langer, W.D. 1997, ApJ, 486, 316

Cecchi-Pestellini, C., & Dalgarno, A. 2000, MNRAS, 313, L6

Elmegreen, B. G. 1999, ApJ, 527, 266

Evans, N. J. 1989, RevMexAA, 18, 21

Evans, N. J. 1999, ARA&A, 37, 311

Falle, S. A. E. G. 2002, ApJ, 577, L123

Falle, S. A. E. G., & Hartquist, T. W. 2002, MNRAS, 329, 195

Garrod, R. T., Williams, D. A., Hartquist, T. W., Rawlings, J. M. C., & Viti, S. 2005, MNRAS, 356, 654

Hartquist, T. W., Falle, S. A. E. G., & Williams, D. A. 2003, Ap&SS, 288, 369

Hartquist, T. W., Williams, D. A., & Viti, S. 2001, A&A, 369, 605

Morata, O., Estalella, R., López, R., & Planesas, P. 1997, MNRAS, 292, 120

Morata, O., Girart, J. M., & Estalella, R. 2003, A&A, 397, 181

Morata, O., Girart, J. M., & Estalella, R. 2005, A&A, 435, 113

Myers, P. C., Fuller, G. A., Goodman, A. A., & Benson, P. J. 1991, ApJ, 376, 561

Peng, R., Langer, W. D., Velusamy, T., Kuiper, T. B. H., & Levin, S. 1998, ApJ, 497, 842

Rawlings, J. M. C., Hartquist, T. W., Menten, K. M., & Williams, D. A. 1992, MNRAS, 255, 471

Rawlings, J. M. C. 19, QJRAS, 37, 503

Sepúlveda Cerrada, I. 2001, PhD Thesis, Universitat de Barcelona

Tafalla, M., Myers, P. C., Caselli, P., Walmsley, C. M., & Comito, C. 2002, ApJ, 569, 815

Taylor, S. D., Morata, O., & Williams, D. A. 1996, A&A, 313, 269

Ungerechts, H., Bergin, E. A., Goldsmith, P. F., Irvine, W. M., Schloerb, F. P., & Snell, R. L. 1997, ApJ, 482, 245

Whittet, D. C. B., Gerakines, P. A., Hough, J. H., & Shenoy, S. S. 19, ApJ, 547, 872

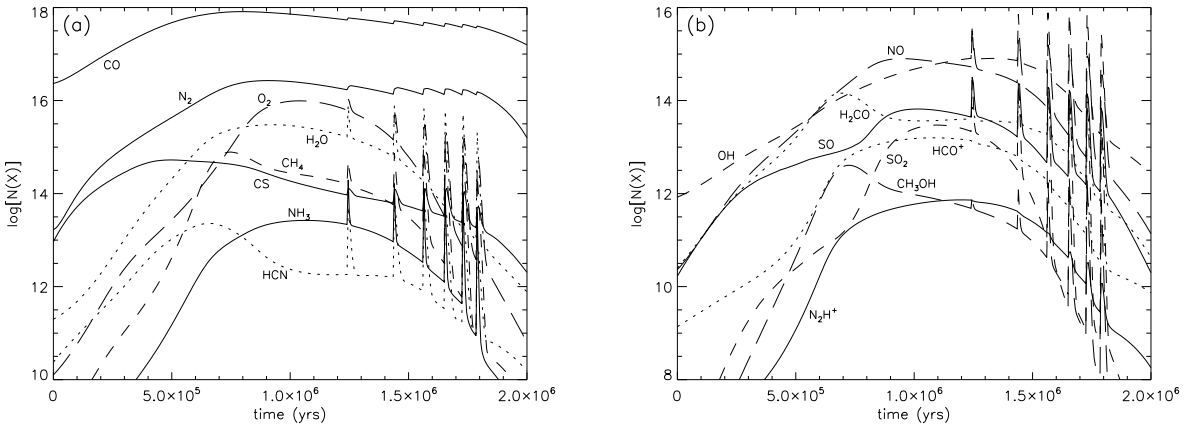

Fig. 1.— Column densities of selected species as functions of time.

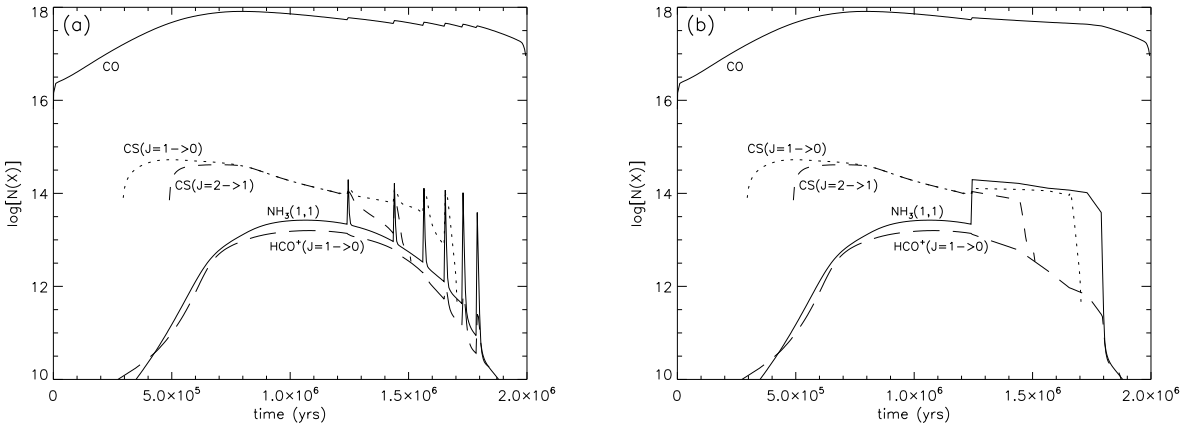

Fig. 2.— Column densities of selected transitions as functions of time, with n_{eff} considerations – (a) unsmoothed and (b) smoothed assuming maximal re-injection.

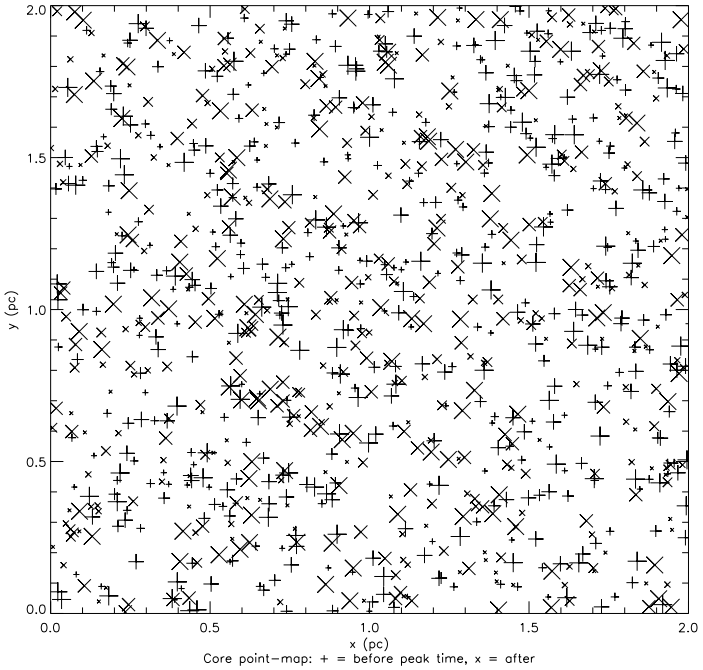

Fig. 3.— Core positions in the basic "sky" map. '+' indicates a pre-peak density core, 'x' indicates a post-peak density core. Symbol size indicates proximity to peak density time, occurring halfway through core evolution.

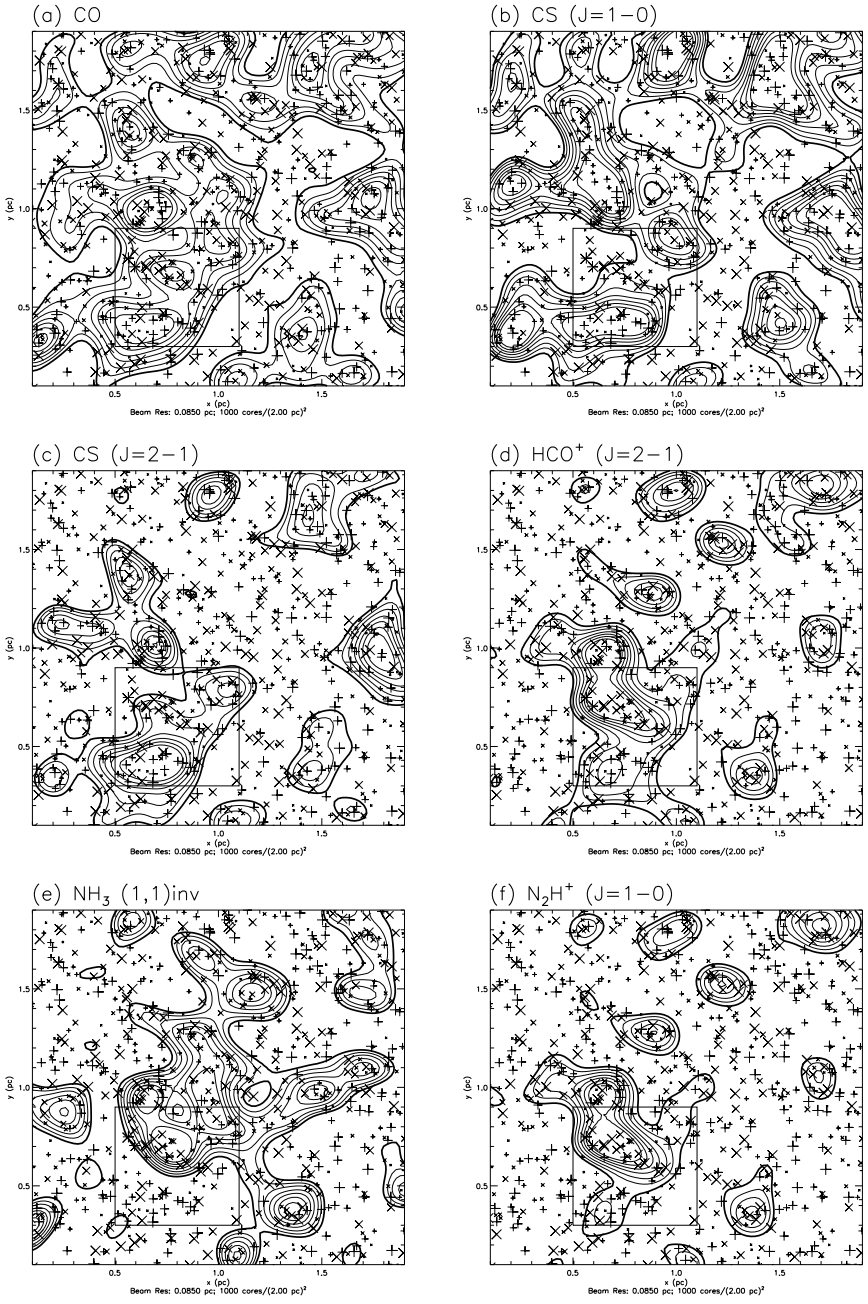

Fig. 4.— Low resolution convolved maps, beam FWHM= 0.17 pc. Maps are trimmed by approximately 1 beam radius to remove effect of artificial map edge in the contour plots. Box in lower left indicates zoomed region shown in figure 5.

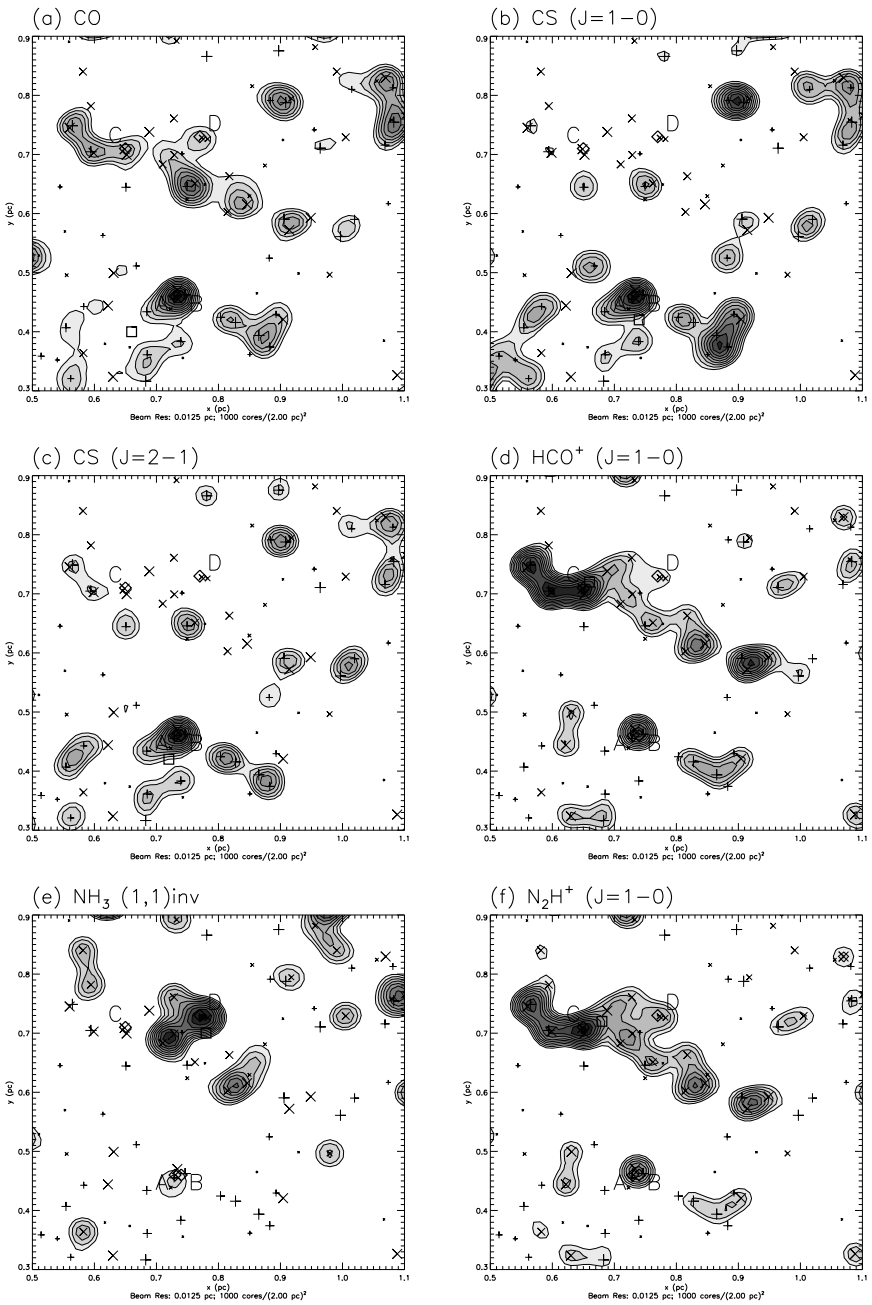

Fig. 5.— High resolution zoomed maps, beam FWHM= 0.025 pc. Map region corresponds to boxed area in figure 4. Square symbol indicates low resolution peak of mapped molecule. Diamond symbols correspond to high resolution peaks in: (A) CO, CS (J=1→0); (B) CS (J=2→1); (C) HCO^+ (J=1→0); (D) NH_3 (1,1)inv.

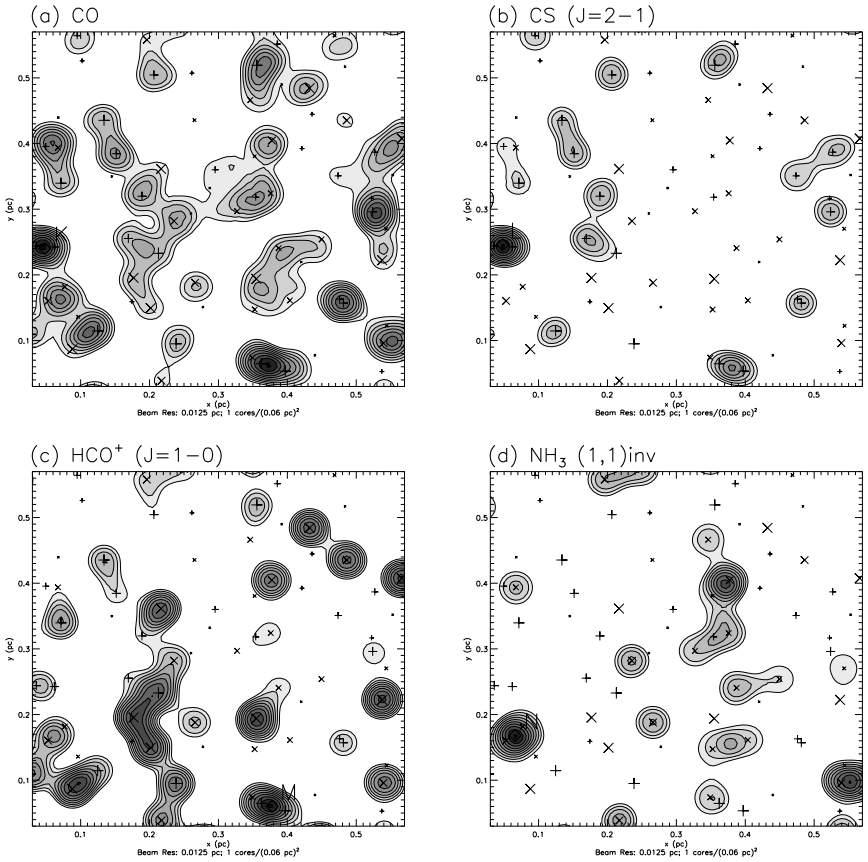

Fig. 6.— Core distribution 1, high resolution, beam FWHM= 0.025 pc. Diamond symbols correspond to high resolution peaks in: (K) CO; (L) CS (J=2→1); (M) HCO^+ (J=1→0); (N) NH_3 (1,1)inv.

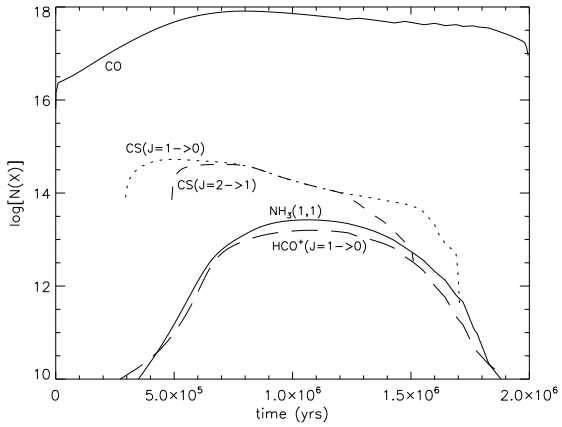

Fig. 7.— Column densities of selected transitions as functions of time, with n_{eff} considerations. Profiles are smoothed assuming minimal re-injection.

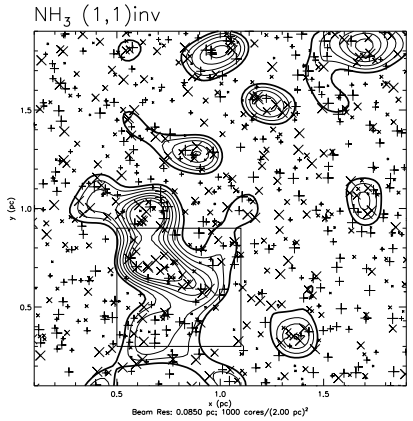

Fig. 8.— Low resolution convolved map, with minimal re-injection, beam FWHM= 0.17 pc.

Table 1. Properties of Line Transitions Utilised in Column Density Calculations

Molecule	Transition	ν (GHz)	n_c(10 K) (cm^{-3})	n_{eff} (10 K) [a] (cm^{-3})
CS	$J = 1 \rightarrow 0$	49.0	4.6×10^4	7.0×10^3
CS	$J = 2 \rightarrow 1$	98.0	3.0×10^5	1.8×10^4
HCO^+	$J = 1 \rightarrow 0$	89.2	1.7×10^5	2.4×10^3
N_2H^+ [b]	$J = 1 \rightarrow 0$	93.2	1.7×10^5	2.4×10^3
NH_3	(1,1)inv	23.7	1.8×10^3	1.2×10^3
CO	—	—	—	1.0×10^3

[a]All values taken from Evans (1999), except CO taken from Ungerechts et al. (1997)

[b]N_2H^+ adopts critical density values given for HCO^+

Table 2. Peak Column Densities for Synthetic Maps

Molecule	Transition	x (pc)	y (pc)	$N[i]$ [a] (cm^{-2})	Peak [b]
CO	—	0.66	0.40	6.0(17)	Low Res
		0.73	0.46	2.2(18)	**Hi − A**
		0.74	0.46	2.2(18)	Hi – B
		0.65	0.71	1.2(18)	Hi – C
		0.77	0.73	1.0(18)	Hi – D
CS	J=1→0	0.74	0.42	2.4(14)	Low Res
		0.73	0.46	9.2(14)	**Hi − A**
		0.74	0.46	9.1(14)	Hi – B
		0.65	0.71	2.4(14)	Hi – C
		0.77	0.73	2.3(14)	Hi – D
CS	J=2→1	0.72	0.42	1.8(14)	Low Res
		0.73	0.46	7.5(14)	Hi – A
		0.74	0.46	7.6(14)	**Hi − B**
		0.65	0.71	2.4(14)	Hi – C
		0.77	0.73	1.1(14)	Hi – D
HCO^+	J=1→0	0.66	0.72	7.5(12)	Low Res
		0.73	0.46	2.4(13)	Hi – A
		0.74	0.46	2.5(13)	Hi – B
		0.65	0.71	2.8(13)	**Hi − C**
		0.77	0.73	1.2(13)	Hi – D
NH_3	(1,1)inv	0.78	0.70	7.9(13)	Low Res
		0.73	0.46	1.4(14)	Hi – A
		0.74	0.46	1.2(14)	Hi – B
		0.65	0.71	4.7(13)	Hi – C
		0.77	0.73	3.1(14)	**Hi − D**
N_2H^+	J=1→0	0.68	0.72	3.6(11)	Low Res
		0.73	0.46	9.3(11)	Hi – A
		0.74	0.46	9.6(11)	Hi – B
		0.65	0.71	1.3(12)	**Hi − C**
		0.77	0.73	7.4(11)	Hi – D

[a] $a(b) = a \times 10^b$

[b] High resolution peaks in bold correspond to the peak in the given transition. Low resolution peak positions are different for each transition.

Table 3. Peak Column Densities from Low and High Resolution Morata et al. Observations

Molecule	Transition	$N[i]$ [a] (cm^{-2})	Peak [b]
CS	J=1→0	2.5(13)	M97 – Low Res
CS	J=2→1	1.20(12) – 2.69(12)	M03 – S
		2.53(12) – 8.48(12)	**M03 – E**
		3.72(12) – 9.96(12)	**M03 – W**
		2.71(12) – 7.22(12)	M03 – N
HCO^+	J=1→0	<4.73(11)	M03 – S
		<3.60(11)	M03 – E
		4.7(11) – 7.7(11)	M03 – W
		7.7(11) – 1.91(12)	**M03 – N**
NH_3	(1,1)inv	≥2.2(14)	M97 – Low Res
N_2H^+	J=1→0	2.2(11) – 3.1(11)	**M03 – S**
		1.7(11) – 2.4(11)	M03 – E
		<2.0(11)	M03 – W
		<1.6(11)	M03 – N

[a] $a(b) = a \times 10^b$

[b] Values are taken from Morata et al. (1997) and Morata et al. (2003). High resolution peaks in bold correspond to the peak in the given transition. Low resolution peak positions are different for each transition.

Table 4. Peak Column Densities for Maps of Various Levels of Uniformity of Core Distribution

Molecule	Transition	Distribution	x (pc)	y (pc)	$N[i]$ [a] (cm^{-2})
CO	—	1	0.048	0.240	1.4(18)
(Peak K)		2	0.186	0.456	1.5(18)
		3	0.390	0.210	2.0(18)
CS	J=2→1	1	0.048	0.246	6.8(14)
(Peak L)		2	0.090	0.030	6.1(14)
		3	0.390	0.210	1.0(15)
HCO^+	J=1→0	1	0.378	0.060	1.7(13)
(Peak M)		2	0.384	0.480	2.5(13)
		3	0.066	0.486	2.0(13)
NH_3	(1,1)inv	1	0.066	0.168	2.9(14)
(Peak N)		2	0.384	0.474	3.2(14)
		3	0.480	0.294	3.0(14)

[a] $a(b) = a \times 10^b$